remote sensing

MDPI

Technical Note

Consolidating ICESat-2 Ocean Wave Characteristics with CryoSat-2 during the CRYO2ICE Campaign

Bjarke Nilsson [1,*], Ole Baltazar Andersen [1], Heidi Ranndal [1] and Mikkel Lydholm Rasmussen [2]

[1] National Space Institute, Technical University of Denmark, Elektrovej 327, 2800 Kongens Lyngby, Denmark; oa@space.dtu.dk (O.B.A.); hvil@space.dtu.dk (H.R.)
[2] DHI GRAS, Agern Alle 5, 2970 Hørsholm, Denmark; mlra@dhigroup.com
* Correspondence: s180866@student.dtu.dk

Abstract: Using the Ice, Cloud, and land Elevation Satellite 2 (ICESat-2) global high-resolution elevation measurements, it is possible to distinguish individual surface ocean waves. With the vast majority of ocean surveying missions using radar satellites, ICESat-2 observations are an important addition to ocean surveys. ICESat-2 can also provide additional observations not possible with radar. In this paper, we consolidate the ICESat-2 ocean observations by comparing the significant wave height (SWH) with coincident CryoSat-2 radar observations during the CRYO2ICE campaign from August 2020 to August 2021. We use 136 orbit segments, constrained to the Pacific and Atlantic oceans as well as the Bering Sea, to compare observations to show the level of agreement between these systems. Three models based on ICESat-2 are used in the comparison: the standard ocean data output (ATL12), a method of modeling the individual surface waves using the geolocated photons and, functioning as a baseline, an approach using the standard deviation of the ocean surface. We find the following correlations between the SWHs from the models and the SWHs from CryoSat-2: 0.97 for ATL12, 0.95 for the observed waves model, and 0.97 for the standard deviation model. In the same comparison, we find mean differences relative to the observed SWHs for each model, as well as errors, which increase as the SWH increases. The SWH observed from ICESat-2 is found to agree with observations from CryoSat-2, with limitations due to changes in the sea state between the satellite observations. Observing the individual surface waves from ICESat-2 can therefore provide additional observed properties of the sea state that can be used alongside other global observations.

Keywords: ocean altimetry; significant wave height (SWH); CRYO2ICE; ICESat-2; CryoSat-2

check for updates

Citation: Nilsson, B.; Andersen, O.B.; Ranndal, H.; Rasmussen, M.L. Consolidating ICESat-2 Ocean Wave Characteristics with CryoSat-2 during the CRYO2ICE Campaign. *Remote Sens.* **2022**, *14*, 1300. https://doi.org/10.3390/rs14061300

Academic Editor: Sergei Badulin

Received: 16 February 2022
Accepted: 6 March 2022
Published: 8 March 2022

1. Introduction

Observing ocean surface waves is a key element in several fields, from understanding the underlying mechanics of waves in climatology to risk assessment in marine engineering [1]. The ability to predict the behavior of ocean waves has increased over the past 30 years due to the use of satellite-based observations [1]. The behavior of ocean waves is complex, and most of them would be too inaccessible for monitoring if not for these space-based altimetry missions. Since TOPEX/Poseidon launched in 1992, the majority of the ocean observation satellites have been using radar altimeters, with more modern missions increasing in precision, which has helped to map the ocean's surface. However, while the ocean surface is observed with a high accuracy, the ocean surface waves are by necessity evaluated using the surface variance, as the radar altimeters have footprints ranging between 1 and 10 km in diameter [2]. By utilizing a high-spatial-resolution laser altimeter from the Ice, Cloud, and land Elevation Satellite 2 (ICESat-2), it is possible to observe small-scale wind waves globally, and not just at the locations of wave stations or on the routes of ships [3]. However, to be able to use these observations in addition to the observations from multi-year missions based on radar altimeters, this method must be compared to current methods. Multi-mission comparisons between satellite altimeters have been done for many missions and are essential for continuous time-series observations, as well as for the calibration and verification of measurements [2,4,5]. To be able to assess the deviation between CryoSat-2 and ICESat-2, we therefore validate CryoSat-2 with multiple satellites at crossover points, as well as with in situ wave measuring stations, to assess eventual biases in observations when validating ICESat-2 measurements.

CryoSat-2 was launched by ESA in 2010 to measure the wind and wave characteristics of the oceans [5]. Because it was launched into a near-polar orbit, with an inclination of 92 degrees and a repeat cycle of 369 days, CryoSat-2 is able to monitor the surface elevation up to latitudes of 88°. Using the SAR (Synthetic Aperture Radar) Interferometric Radar Altimeter (SIRAL), CryoSat-2 observes the significant wave height (SWH) using the leading edge angle of the return power reflected from the ocean surface [6] at a high spatial resolution compared to conventional systems like the Jason satellites. With a nominal footprint of 15 km, SIRAL observes a larger swath of the ocean surface with each pulse and thereby assesses the sea state.

ICESat-2 uses a different approach. It carries the Advanced Topographic Laser Altimeter System (ATLAS), a photon-counting laser altimeter, and observes surface elevations at up to 88° latitude, similar to CryoSat-2. Launched in 2018 by NASA, it follows the successful ICESat mission, which operated from 2003 to 2009, and allows for high-resolution observations of individual return photons, with a nominal 17 m footprint and a 3×2 beam configuration [7]. Grouping the beams into pairs with a nominal intermediate distance of $\sim$3.3 km allows ICESat-2 to measure elevation changes along the ground track. Designed to measure changes in ice thickness as well as vegetation canopy heights, ICESat-2 also provides ocean surface topography data [8].

Studies comparing data from both the radar altimeter on CryoSat-2 and the laser on ICESat-2 have previously been limited to crossover events separated by varying time lags and longer overlaps closer to the poles [9]. As a result, the feasibility and benefits of adjusting the orbit of CryoSat-2 to repeatedly overlap with ICESat-2 were acknowledged [9,10]. This was achieved in July 2020 with the CRYO2ICE campaign [11]. CRYO2ICE is designed to produce repeated overlaps (every 19th CryoSat-2 and 20th ICESat-2 revolution) of extended time (>30 s of overlap), allowing for several near-simultaneous observations of the same surface using both radar and laser techniques [12]. This is especially useful when observing the ocean's surface topography due to its high variability. By 1 August 2021, one year of passes had been collected, so that there were enough data to compare the two altimeter systems [13].

Here, we focus on the open ocean, where [3] has assessed the feasibility of using ICESat-2's photon-counting lidar to determine wave and wind characteristics with a high spatial resolution and thereby model the individual surface waves. The ability to observe individual surface waves along a ground track that is also being monitored by a radar altimeter would provide additional knowledge about the ocean surface, such as peak wave heights and the distribution of wave heights.

2. Data

This section contains an overview of the data products from ICESat-2 and CryoSat-2, as well as the corrections made to CryoSat-2, which were determined from a comparison with in situ observations. A comparison between CryoSat-2 and Sentinel-3A/B and SARAL is also done to assess the behavior of CryoSat-2.

2.1. ICESat-2 Data

ICESat-2 data has been provided by the National Snow and Ice Data Center (NSIDC). The database contains all released data products for the ICESat-2 mission; version 4 is used in this study. The ATLAS [7] data used includes the ATL03 Global Geolocated Photon Data [14] and ATL12 Ocean Surface Height [8] data products.

ATL03 contains observations of each individual photon event and is used as the basis of higher-level data products produced for the ICESat-2 mission (such as ATL12). ATLAS operates at 10 kHz, which corresponds to a ∼0.7 m along-track nominal spacing. In this study, ATL03 is used to produce the models used in Section 3. ATLAS uses six beams to measure elevation, although three of them, designated the strong beams, have four times the energy of the weaker beams [14]. This is the nominal configuration; however, when the ocean surface is observed, only the strong beams are used to collect observations due to the lower reflection of the ocean surface compared with ice sheets [15]. The surface type is provided as a standard output of ATL03 and is used as a rough filter for surface ice and other surface types. We have used the ATL03 data to produce models estimating the significant wave height; these models are described in Section 3 (Methods). A detailed description of the data can be found in the data user guide at (https://nsidc.org/data/ATL03/versions/4, accessed on 26 August 2021).

ATL12 contains the SWH product used in this study. The along-track spacing of the ATL12 data is variable, between 70 m and 7 km. This spacing is therefore highly dependent on the weather conditions [8]. Version 4 of the data includes a bathymetric depth test for the data, thereby allowing one to exclude data when the depth is shallower than 10 m, according to the General Bathymetric Chart of the Oceans (GEBCO), to include only ocean waters [16]. As ATL12 is the standard data output for the significant wave height, no change has been made to this output. There is a short description of the method used to estimate the SWHs in ATL12 in Section 3 (Methods). A detailed description of the data can be found in the data user guide at (https://nsidc.org/data/ATL12/versions/4, accessed on 26 August 2021).

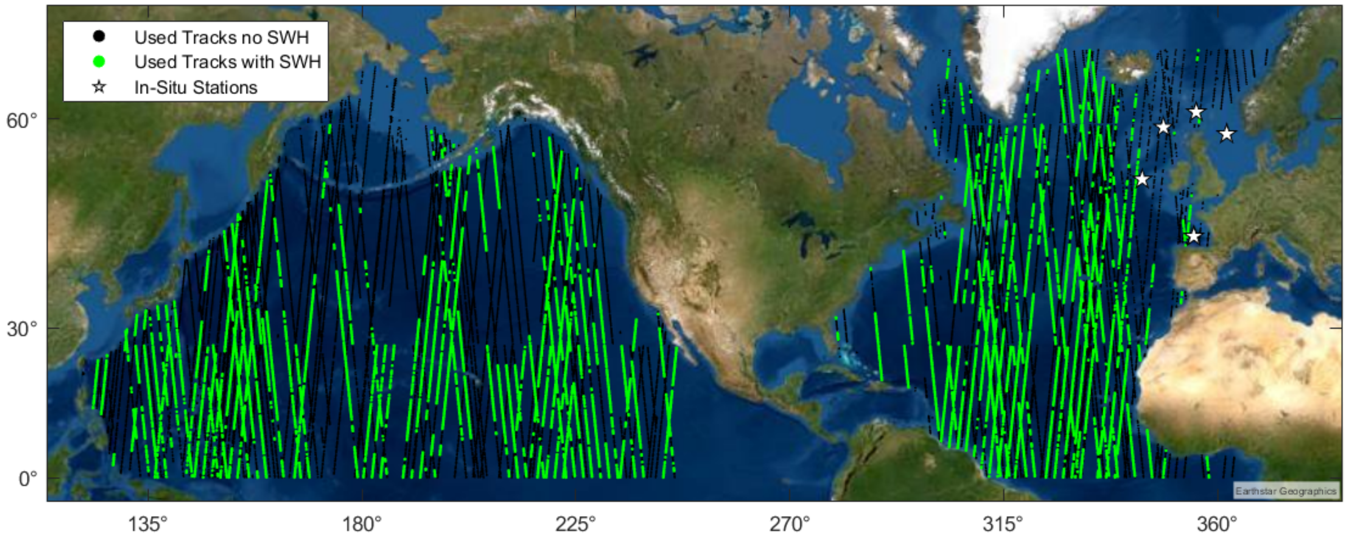

Figure 1. CryoSat-2 orbits (black) in the Pacific and Atlantic oceans, as well as the Bering Sea, for the period from 1 August 2020 to 1 August 2021, that are coincident with ICESat-2 and contain wave height measurements (green). 136 CryoSat-2 orbits from this period have been found to be both coincident with ICESat-2 and more than 40 km from land. The analysis has been limited to latitudes between 0 and 70 degrees north. White stars indicate the locations of the in situ stations used to validate the CryoSat-2 data.

2.2. CryoSat-2 Data

The radar altimeter on CryoSat-2 makes observations in the Ku-band using different sampling modes. The observation mode of SIRAL switches between the low-resolution mode (LRM), synthetic aperture radar (SAR) mode, and SAR interferometric mode according to a geographical mode mask [6]. In this study, we use data from the Radar Altimeter Database System (RADS), which is maintained by the Delft Institute for Earth-Oriented Space Research [17]. Along with times and locations, the 1 Hz significant wave height is provided for use in this study. To obtain a consistent dataset throughout the ocean regions where SIRAL was operating in SAR mode, RADS converts the data to "Pseudo-LRM" data, providing the 1 Hz measurements with a 15 km footprint that are used in this study [18,19].

2.3. In Situ CryoSat-2 Correction

As CryoSat-2 has been in operation for a longer amount of time than ICESat-2, we are able to compare ICESat-2 SWH observations across the oceans with validated CryoSat-2 observations at in situ stations for a longer time series. We have compared CryoSat-2 with in situ station observations from 31 July 2010 (corresponding to CryoSat-2 cycle 005) to 21 May 2021 (corresponding to CryoSat-2 cycle 144). Validation with in situ stations has been carried out at five locations, which are depicted as white stars in Figure 1, with data from the North-West Shelf Data Portal [20]. The stations are located at ocean depths greater than 1 km, except one station in the North Sea that is located at a depth of 96 m. Information on the stations used is listed in Table A1 in the Appendix A. Observations from CryoSat-2 are used if they are closer than 50 km to the station location, and the average SWH is computed for each pass, which gives 2124 observations below 12 m. The in situ stations record wave heights continuously, and from this time series, the SWH is determined for every hour. The maximum time difference between the in situ stations and CryoSat-2 is therefore one hour.

The resulting validation of CryoSat-2 using the in situ stations can be seen in Figure 2, which shows fairly good agreement between CryoSat-2 and the in situ stations, with a correlation of 0.983 and a root mean squared error (RMSE) of 0.308 m. The red points plotted in Figure 2 are the 0.1%-quantiles of the in situ station SWH observations. They are plotted against the same quantiles determined using CryoSat-2, and the plot shows good agreement between the two data sources. In the following comparison with ICESat-2, the CryoSat-2 data is corrected with reference to the linear fit between the observations. The linear fit used is $SWH_{CS2-corrected} = 1.026 \cdot SWH_{CS2} - 0.068$ because the in situ data are used as a baseline for the fit. This correction is done to allow for a better validation of the altimeter measurements of ICESat-2.

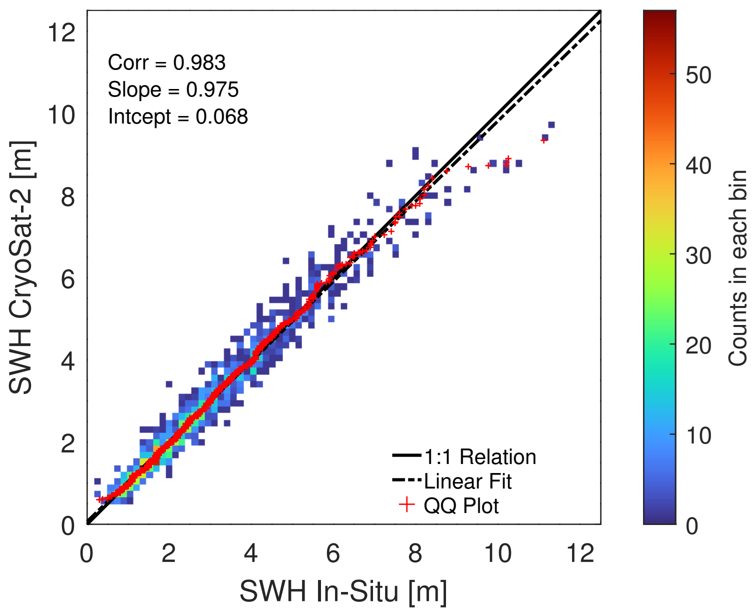

Figure 2. Comparison of CryoSat-2 significant wave height (SWH) observations and in situ stations to show any bias or change in the altimeter measurements compared to the true measured data. Using 2124 observations, a mean difference of −0.009 m and an root mean squared error (RMSE) of 0.308 m were found.

2.4. Satellite Altimeter Crossover Validation

As the in situ comparison is inherently restricted in its ability to validate CryoSat-2 due to geographical limitations, we compare CryoSat-2 to several other satellite altimeters to see if there are discrepancies between the observations. The satellites used in the comparison are the Sentinel-3A and B as well as the SARAL. Together they span most of the operational time of CryoSat-2, with Sentinel-3B spanning about the same amount of time that ICESat-2 has been operational. The comparison is done at crossover points determined by the RADS radsxogen library [17]. At points in time when CryoSat-2 and one of the other satellites cross each other, the observations from each satellite are saved, and the time difference is registered. The resulting metrics from the analysis are summarized in Table 1; the un-corrected CryoSat-2 data is used.

Table 1. SWH measurements from Sentinel-3A, Sentinel-3B, and SARAL compared with CryoSat-2. Here, the time separation increases by one-hour intervals up to a three-hour time separation to show the decrease in correlation and increase in root mean squared error (RMSE).

Time Sep. [H]	Sentinel-3A				Sentinel-3B				SARAL			
	Diff. [m]	RMSE [m]	Corr	N	Diff. [m]	RMSE [m]	Corr	N	Diff. [m]	RMSE [m]	Corr	N
0–1	0.106	0.188	0.995	11,466	0.117	0.198	0.995	7237	0.003	0.130	0.996	16,512
1–2	0.086	0.232	0.990	13,834	0.100	0.239	0.990	8664	0.002	0.178	0.993	19,259
2–3	*0.105*	*0.292*	*0.983*	*11,358*	*0.116*	*0.294*	*0.984*	*6602*	*0.003*	*0.254*	*0.985*	*16,140*
0–3	0.092	0.308	0.981	66,253	0.100	0.308	0.981	39,711	0.002	0.269	0.983	90,500
Data interval:	1 March 2016 to 24 January 2022				8 May 2018 to 25 January 2022				14 March 2013 to 26 January 2022			

As can be seen in the table, the satellites have very high correlations and low errors when observations that are close together in time are compared, and the correlation decreases as the time difference between the observations increases. A comparison for each of the satellites can be seen in the scatterplots in Figure 3, which includes observations with a time lag of between two and three hours; thus, we have a slightly larger variance than we would have if we showed a scatterplot of observations with time lags of less than one hour. This time lag, as shown in Figure 3, is important, as it corresponds to the time difference between ICESat-2 and CryoSat-2 in the CRYO2ICE campaign. The same Q-Q plot shown for the in situ stations in Figure 2 is shown in Figure 3 for each of the altimeters, and we can see that the altimeters show good agreement with each other.

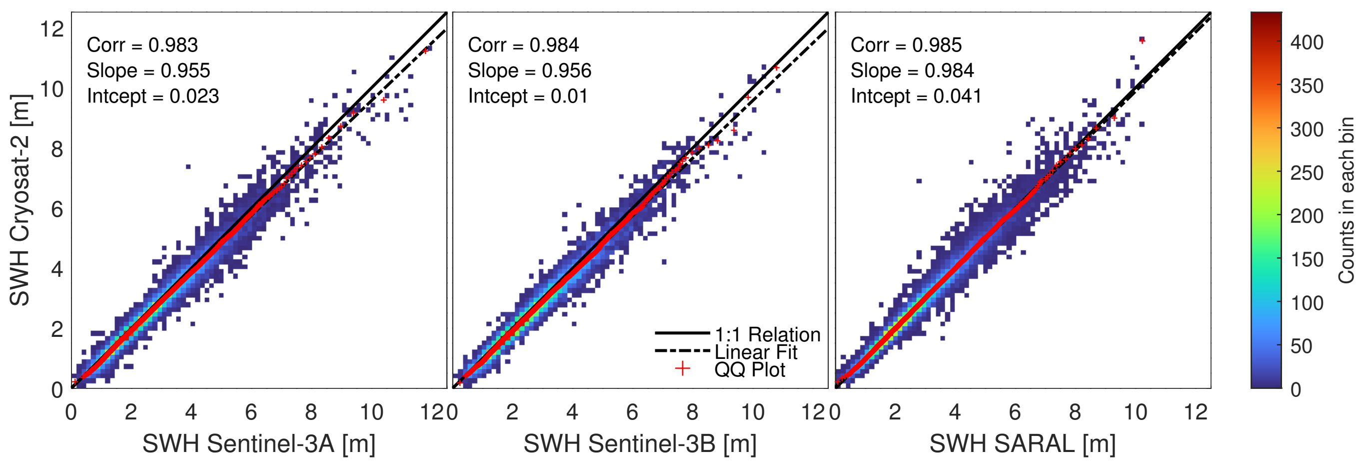

Figure 3. Crossover analysis for three altimeters and CryoSat-2 showing the agreement between SWH observations for crossovers with a time difference of between 2 and 3 h. The correlations are also shown in Table 1; we expect correlations in this range.

2.5. CRYO2ICE Orbit Matching

The extent of the study is limited to the coincident orbits following the orbit change of CryoSat-2 in 2020. The matching of the coincident orbits between ICESat-2 and CryoSat-2 has been carried out using the (cryo2ice.org, accessed on 10 August 2021) coincident data explorer [21]. 547 coincident orbits were found from 1 August 2020 to 1 August 2021, in the region from 0° to 70° N, with 168 orbits containing ocean observations within the set limits. The rejected orbits were primarily short-time (<3 s) measurements containing land observations, with only the long-time coincident orbits reaching the open ocean for the most part.

We decrease the 168 orbits to 136 orbits containing observations from the Pacific or Atlantic oceans, including the Bering Sea, that are at least 40 km from land. This limits shallow-water wave effects [22], as well as noise from photons reflected by the ocean floor [23]. A map showing the orbits used in this study can be seen in Figure 1. The location for each measurement has been designated using the National Oceanic and Atmospheric Administration (NOAA) basin codes, which were obtained from the RADS database [24]. The matching orbits have been limited to allow for a maximum separation of 50 km between ground tracks, with generally larger separations at lower latitudes; however, no significant increase in the RMSE was found with larger separation distances below the 50 km limit. Due to the configuration of the orbits, the time difference of the observations is between 2.3 h and 3 h, with an average time difference of 2.8 hours.

3. Methods

In this section we describe the different models applied to the ICESat-2 data to assess the performance of ICESat-2 by comparing the significant wave heights from the models to the significant wave heights obtained from SIRAL (the radar altimeter carried by CryoSat-2).

3.1. CryoSat-2

Functioning as a conventional radar altimeter system, CryoSat-2 measures the leading edge of the return waveform to assess the SWH; here, the SWH is averaged over 14 km along the ground track [6]. As the reflected signal hitting the wave crest is returned earlier than the reflected signal hitting the wave trough, the height of the wave can be inferred from the time difference between the earliest and latest returns of the reflected signal. Frequently, when using altimetry measurements, multiple geophysical corrections are applied; as only the wave heights are of interest in this study (corresponding to a height difference), no corrections other than the corrections discussed in the previous section have been used.

3.2. ATL12 SWH

The ocean data product of the ICESat-2 mission, ATL12, contains the statistical properties of the ocean surface determined from the ATL03 photon data [8]. Using both low-, medium-, and high-confidence photons classified by the ATLAS photon classification algorithm [14] and a hard buffer limit of ± 15 m around the EGM2008 geoid, each point along the ground track is accumulated, and a linear fit is made to account for local drift. The accumulated data is fitted with a Gaussian mixture model to assess the first four statistical moments of the distribution of surface heights [8]. The second statistical moment is the variance (m_0); however, in ATL12, the second moment is provided as four times the standard deviation. Using the following relationship, the SWH can be calculated directly from the data product: $\mathrm{SWH} = 4\sqrt{m_0}$.

3.3. ATL03

Two models are made in this study using the ATL03 geolocated photons: one model finds the ocean surface to determine the waves, and another uses the same basic principles as ATL12 to act as a baseline.

3.3.1. Histogram Model

The significant wave height approximately follows a Rayleigh distribution ($p_H(H)$) in deep water scenarios, with a probability density function (PDF) of

$$p_H(H) = \frac{H}{4m_0} \exp\left(-\frac{H^2}{8m_0}\right), \tag{1}$$

where H is the wave height and m_0 is the variance of the ocean surface [1]. As the SWH is defined as the average of the highest one-third of the waves, calculating it requires the individual surface waves to be distinguished. This is not always possible; therefore, the corresponding cumulative distribution function (CDF) of the Rayleigh distribution can be evaluated to provide the relationship SWH $= 4\sqrt{m_0}$, and therefore only the variance of the surface needs to be known [1].

The high-resolution laser data from ATLAS enables us to observe the individual surface waves of the ocean and thereby establish an assessment of the SWH using the distribution of the individual surface waves; this method is described in [3]. This method of using each return photon event as an individual surface measurement requires robust filtering and model fitting to reconstruct the measured "ground" surface, as seen in Figure 4.

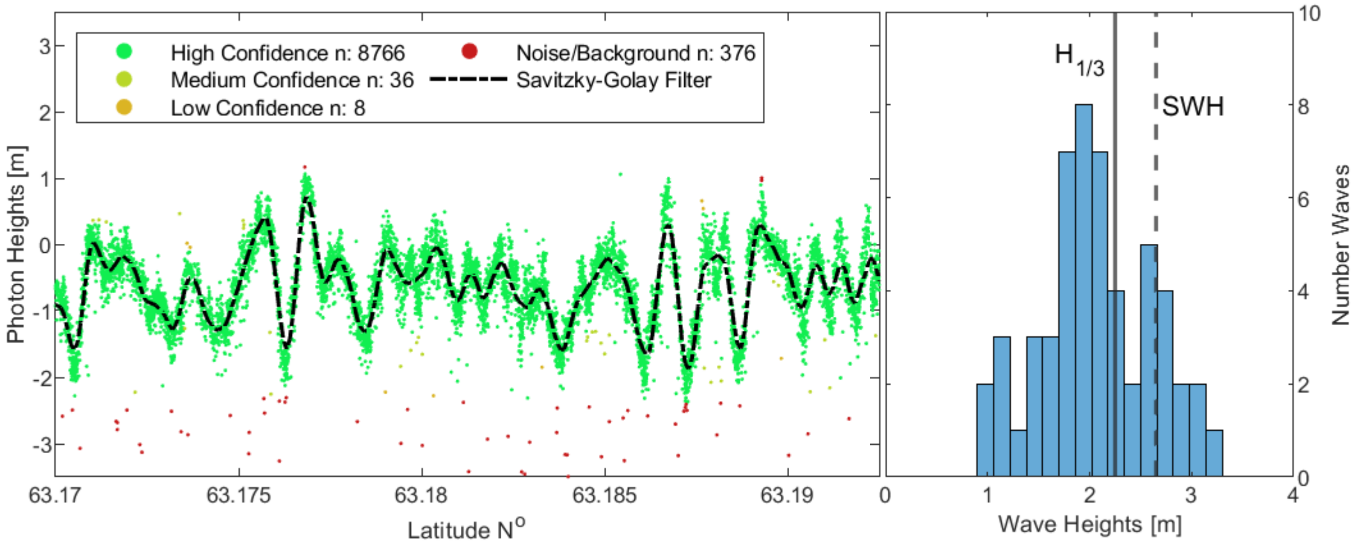

Figure 4. (**Left**) Scatterplot of the geolocated surface photons along a segment of a ground track (∼2.5 km along the surface) of ICESat-2 granule 10460805 beam GT3L. (**Right**) Histogram of the observed ocean wave heights showing the locations of the highest 1/3 ($H_{1/3}$) of wave heights and the corresponding SWH for the 10 km segment starting at the latitude 63.17° N.

The ground tracks are divided into 10 m along-track segments and are thereafter filtered with a hard limit of ±20 m from the EGM2008 geoid, and photon heights that are ±3 σ from the mean in each 10 m bin are also filtered out. The data are subsequently fitted with a smoothing Savitzky–Golay filter, which preserves the peak amplitudes of the signal while smoothing the noisy data. If there are missing data in less than four consecutive 10 m bins, the data are fitted with a local spline before the smoothing filter is applied. The crests and troughs are thereafter located while correcting for the distribution of photons around the mean (to establish a 0 m height that represents a theoretical calm sea). In 10 km segments with 500 m of overlap, the wave heights are then sorted by height, and the mean of the highest one-third of the waves is then used to estimate the SWH in that section. To check for low amounts of data, a lower limit of at least 15 waves in a segment of 10 km is set; this provides an amount of data coverage comparable to that of ATL12.

As the histogram model derives the SWH from the individual observed surface waves, the wave distribution along the ground track is observed and provides an additional ocean observation output. For the single granule of ICESat-2 data (ID: 10460805) shown in Figure 4, that is, for a segment of 10 km (only ∼2.5 km of which is shown in the left plot), 54 individual waves were found from a single beam; they have an SWH of 2.66 m, a maximum wave height of 3.26 m, and a minimum wave height of 0.9 m.

3.3.2. Standard Deviation Model

The standard deviation model uses the same characteristic of the significant wave height as ATL12, that is, $SWH = 4\sqrt{m_0}$, and forms a baseline model for the more complex histogram model that assesses the SWH directly from the individual waves. This method uses the same filtering and spacing of the segments as the histogram model and can therefore be used to assess the histogram approach. While this method uses the same approach as ATL12, the filtering and sequencing process is the same as the filtering and sequencing process of the histogram model; the limit on the number of waves is replaced by a limit of at least five photons per 10 m segment.

4. Results

Comparisons between the SWHs determined from CryoSat-2 and the ICESat-2 derived models are presented in this section. The full dataset from 2020 to 2021 is used. The wave fitting of each ground track is presented with examples in Section 4.1, and the behavior of the full dataset is shown in Section 4.2. In Section 4.3, the dependency of the models on the sea state is analyzed.

4.1. Orbit Pairing Segmentation

To be able to compare ICESat-2 derived data with CryoSat-2 measurements at different resolutions, the data have been binned in 0.2° segments that are approximately 22.2 km long in the northern direction. Then, the SWH observations are averaged, and the location is set as the mean latitude and longitude of the bin. Some specific tracks with large stretches of data available can be seen in Figure 5. In Figure 5 (top), there are stretches with CryoSat-2 SWH data that are missing from all ICESat-2 models due to clouds, and in Figure 5 (bottom), there are gaps for both satellites due to islands. As CryoSat-2 has been used as the baseline, only tracks with available CryoSat-2 SWH data have been used. By binning all of the models using the same interval, the spatial difference has been taken into account. The 5th, median, and 95th percentiles as well as the maximum heights of the observed waves can be seen in Table 2.

Table 2. Distribution of SWH observations for each model.

	CryoSat-2	**ATL12**	**Histogram Model**	**Standard Deviation Model**
5%	1.01 m	0.89 m	1.07 m	1.11 m
50%	1.96 m	1.76 m	2.06 m	2.07 m
95%	4.96 m	4.32 m	4.70 m	4.82 m
Max.	10.68 m	10.98 m	10.19 m	12.17 m

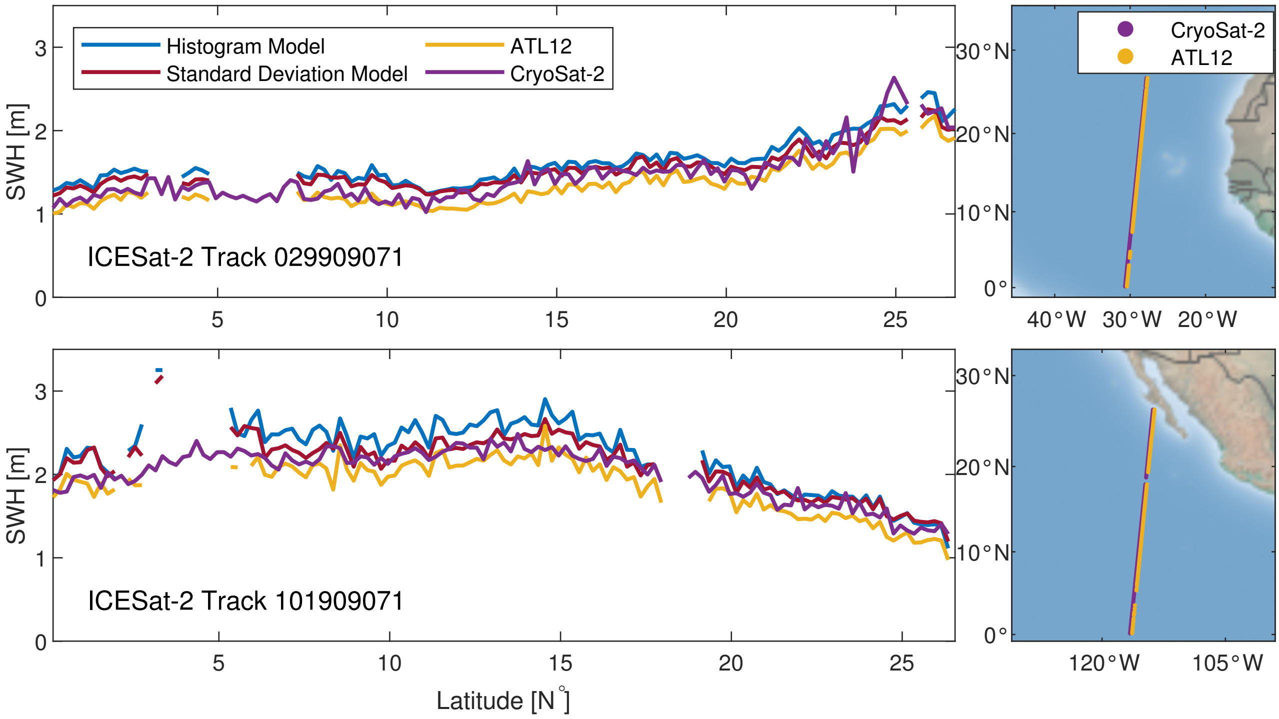

Figure 5. Ground tracks of ICESat-2 orbit segments and the corresponding SWHs for the different models. This plot shows track pass 299 cycle 7 granule 7 (**top**) in the Atlantic Ocean, which has visible gaps for ICESat-2 (due to clouds), and pass 1019 cycle 9 granule 7 (**bottom**) in the Pacific Ocean, which has gaps for both satellites.

4.2. Full Data Comparisons

For the entire year of data, the number of individual observations along the ground tracks is 36763 for ATL12, 37861 for the histogram model, and 37861 for the standard deviation model. CryoSat-2 data are available at each corresponding along-track segment of ICESat-2, as well as for several instances in which ICESat-2 data are obstructed due to clouds. SWHs determined from ICESat-2 and CryoSat-2 show a clear correlation, which can be seen in Figure 6 along with a linear least-squares fit. Some outliers can be seen at 2–3 m for the histogram and standard deviation models; this is due to noisy data. The Q-Q plot clearly shows a deviation below the linear fit to the ATL12 and CryoSat-2 data, whereas the other two models seem to be fairly consistent. To see the effects of the differences between the models and CryoSat-2, we break up all the observations into segments to show these differences as a function of the SWH.

4.3. Sea State Dependency Bias

To analyze the behavior of the models for varying sea states, the RMSE and the mean deviation are determined as functions of the CryoSat-2 SWH. After sorting the observations according to their SWHs, with SWHs from 0 m (calm sea) to 10 m (rough sea), the RMSE and mean deviation of the models from CryoSat-2 are calculated; they can be seen in Figure 7. The observations above 10 m are excluded from this figure because there are too few observations above this height (only three observations above 10 m). As seen in Figure 7A, the RMSE generally increases as the SWH increases. The three models follow each other closely, especially at lower SWHs, with the RMSE being slightly higher for the histogram model until an SWH of approximately 7–8 m is reached; for higher SWHs, the RMSE of the ATL12 product is noticeably higher.

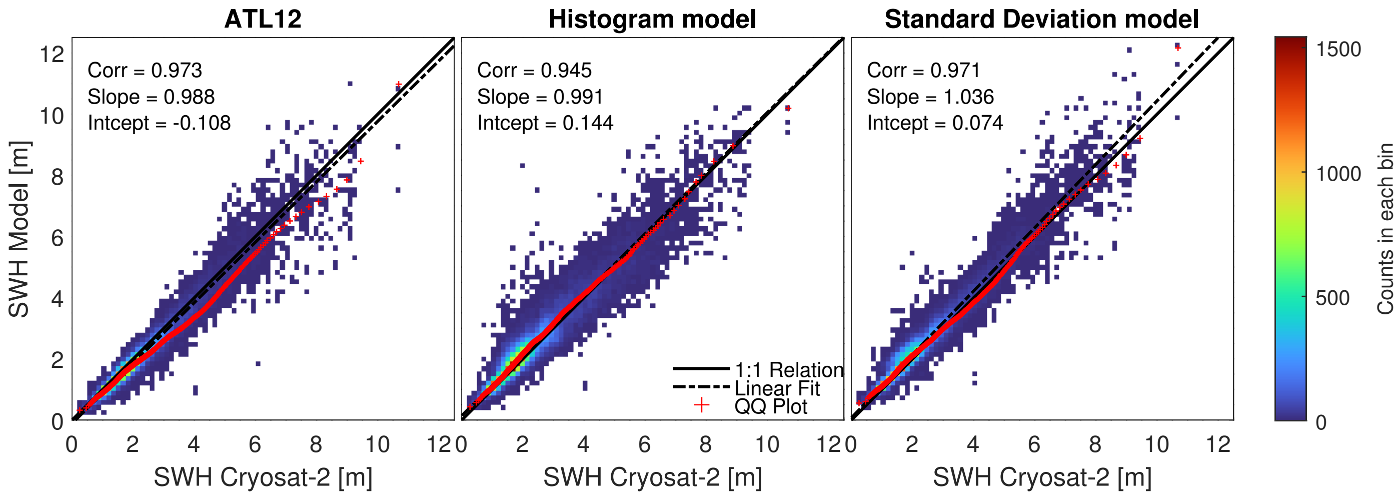

Figure 6. Density plots of the three ICESat-2 models compared to CryoSat-2, with individual points indicating low-density areas. The solid line corresponds to the 1:1 relation, and the dashed line is the least-squares linear fit. There are 36,763, 37,861, and 37,861 data points in the ATL12, histogram, and standard deviation models, respectively. The red points are the Q-Q plots.

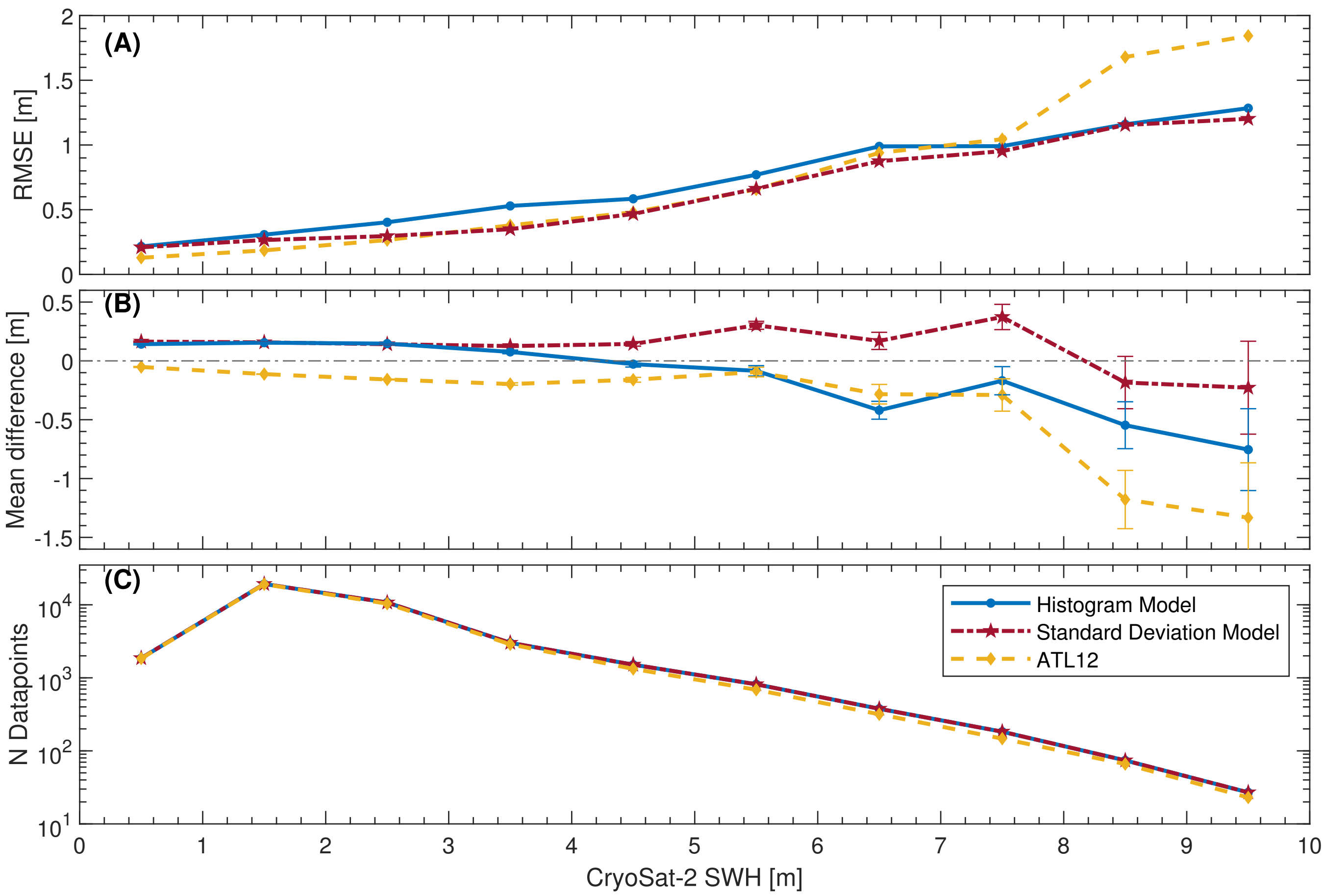

Figure 7. Behavior of the three models compared to CryoSat-2 for increasing SWHs. (**A**) Root mean squared error for each model for increasing SWHs. (**B**) Mean differences between the model SWHs and SWHs determined by CryoSat-2, with 95% confidence intervals at each point determined from the model samples. (**C**) Number of data points at each SWH.

In Figure 7B, the mean difference is shown for each of the models. The mean difference is estimated using the mean of the residuals: res $= \text{SWH}_{model} - \text{SWH}_{CS2}$. Both ATL12 and the standard deviation model have stable biases for SWHs below 8 m, with that of the ATL12 product being slightly negative and that of the standard deviation model being slightly positive. The mean difference of the histogram model is similar to that of the standard deviation model until an SWH of around 4 m is reached; for higher SWHs, the mean difference becomes negative. It is clear that at higher SWHs, all models underestimate the SWH compared to CryoSat-2. The 95% confidence intervals of the mean differences are shown in Figure 7B as error bars. They are calculated using the following expression: mean $\pm\, t(n-1)_{0.95} \cdot \sigma/\sqrt{n}$, where $t()$ is the t distribution, σ is the standard deviation, and n is the number of samples at each indicated point. As shown in Figure 7C, the number of data points available to use for comparison drops for rougher sea states. The number of available data points drops below 100 observations above an SWH of 7 m, and there are many observations available for SWHs between 1 and 3 m.

The model performance metrics are divided into segments of 0–1.5 m, 1.5–2.5 m, and 2.5–11 m. Approximately one-fourth of the SWH observations made by CryoSat-2 are contained in each segment, except that the middle segment has one-half of these observations; the values can be seen in Table 3. The behavior shown in Figure 7 can be seen more prominently in this table, with a positive bias of up to 0.18 m for the histogram model below SWHs of 2.5 m and a lower bias at high SWHs. Meanwhile, the standard deviation model has a better performance, with a lower difference and a lower standard deviation. While the differences between the derived models and CryoSat-2 are positive, ATL12 experiences a mean negative deviation for all segments. The scatter index (SI), which is the RMSE divided by the mean of the segment and converted to a percentage value, is largest at lower measured SWH values, and it decreases for higher SWH values.

Table 3. Mean difference (Diff.), standard deviation (SD), and scatter index (SI) from the comparison between the models and CryoSat-2, as well as the number of data points (N) for each SWH segment.

SWH	0–1.5 m				1.5–2.5 m				2.5–11 m			
Models	**Diff.**	**SD**	**SI**	**N**	**Diff.**	**SD**	**SI**	**N**	**Diff**	**SD**	**SI**	**N**
Histogram	0.18 m	0.23 m	39.5%	9883	0.18 m	0.31 m	17.7%	18,390	0.01 m	0.59 m	8.75%	9583
Standard Deviation	0.19 m	0.19 m	35.7%	9883	0.17 m	0.23 m	14.5%	18,390	0.13 m	0.43 m	6.67%	9583
ATL12	−0.06 m	0.14 m	19.77%	9750	−0.11 m	0.17 m	10.2%	18,225	−0.22 m	0.45 m	7.36%	8788

5. Discussion

The comparison between the histogram model, which fits the high-resolution data of ICESat-2 photons, and the radar CryoSat-2 data gives a correlation of 0.95, with a mean difference of 0.14 m and an RMSE of 0.42 m. The study presented in [3], which compared a model derived from the individual waves observed by ICESat-2 with data from the European Centre for Medium-Range Weather Forecasts, gave a median difference of 0.07 m, correlation of 0.91, and RMSE of 0.38 m. The comparison in [3] has a lower time lag compared to this study; however, it was based on a gridded model. While this method has a higher difference than the methods based on the standard deviation (both ATL12 and the standard deviation model), it shows the possibilities of extracting additional information from surface observations of the oceans. Some effects of the observed waves, such as the wave direction, were corrected for in [3] but were not considered in our study to allow the determination of the SWH without using external tables. The metrics from this study can be seen in Table 4, along with those of the three models used in [3]. ATL08-Ocean is equivalent to the histogram model in this paper, and CryoSat-2 and ATL12 are the standard data output. ATL12 in [3], when ERA-5 is used as a reference, has a comparable performance to ATL12 in this paper, although we found that ATL12 has a more negative bias when it is compared to CryoSat-2.

The overall performance of the different models, independent of the observed wave height, can be estimated using the scatter index, as shown in Table 3. Using all the observations, the SI of the histogram model is 17.6%, and it is 14.2% for the standard deviation model and 12.7% for ATL12. ATL12 overall has fairly good agreement with CryoSat-2, while the other models experience slightly higher errors, but ATL12 deviates in the Q-Q plot. While this could be caused by a larger number of observations at lower SWHs, we have not proved that this is the case. The performance was estimated on the in situ corrected CryoSat-2 data; however, the difference was not large (approximately 3%).

Table 4. Collection of the comparisons done in this study, including the validation of CryoSat-2, comparisons between the methods derived in this paper and CryoSat-2, and the comparison of similar methods with ERA-5 [3] († ATL08-Ocean determines the SWH from the individual surface waves, like the histogram model).

Method	Reference	Mean Diff. [m]	RMSE [m]	Corr.	N
		Validation			
CryoSat-2	In Situ	−0.01	0.31	0.98	2124
CryoSat-2	Sentinel-3A	0.11	0.29	0.98	11,358
CryoSat-2	Sentinel-3B	0.12	0.29	0.98	6602
CryoSat-2	SARAL	0.00	0.25	0.96	16,140
		Method Comparison			
Histogram Model	CryoSat-2	0.14	0.42	0.95	37,861
Standard Deviation Model	CryoSat-2	0.17	0.33	0.97	37,861
ATL12	CryoSat-2	−0.12	0.29	0.97	36,763
		Analysis by [3]			
ATL08-Ocean †	ERA-5	0.07	0.38	0.91	N/A
ATL12	ERA-5	−0.16	0.33	0.95	N/A
CryoSat-2	ERA-5	−0.01	0.36	0.95	N/A

Comparisons with in situ measurement stations have previously been done for multiple satellite missions, with [2] using seven satellite missions in their comparison. Their study showed a high correlation for all missions (above 0.982) and an RMSE between 0.15 and 0.21 m, which is comparable to the crossover comparisons done in this paper (Table 1). However, when using CryoSat-2 as a baseline for ICESat-2, such a high correlation is not possible due to the average time lag between the satellites of 2.8 h, because in this amount of time, the sea state can change significantly. This is clear in Figure 6; however, within the known constraints, the correlations are still just below the expected correlation, as shown by the crossover analysis. A disadvantage of using the observed waves to determine the SWH is the necessity of observing an entire wave or large parts of it. With ocean waves able to reach several hundred meters, larger gaps in the data reduce the number of available waves that can be used to determine the SWH; this could induce a bias toward smaller SWHs for rougher seas, and of course using a small number of waves to determine the SWH will probably result in a bad estimate. While we do find a significant negative difference between ICESat-2 and CryoSat-2 at high SWHs (above 8 m), for the comparison between CryoSat-2 and ICESat-2, we have very few CryoSat-2/in situ observations in this region to use to accurately determine the behavior of CryoSat-2 and ICESat-2 at these SWHs. While there is no clear difference compared to other satellite altimeters, as seen in Figure 3, the difference at this wave height between ICESat-2 and CryoSat-2 cannot be directly validated with in situ data.

A limitation of this study is the use of co-linear orbits containing ocean data that are only located in the Northern Hemisphere. Validating the model for larger SWHs requires enough observations at these wave heights, and although cloud cover is a problem for laser observations because it limits observations of rough seas, observations of the rough seas of the Southern Ocean would be of great importance. However, the co-linear orbits of ICESat-2 and CryoSat-2 drift too far apart at these latitudes under the current orbital configuration and their orbits would need adjustments to allow them to have the same collinearity in the Southern Hemisphere. Further usage of ICESat-2 ocean data will also be of interest when the next radar altimeter satellite, CRISTAL, is launched.

6. Conclusions

Data from CryoSat-2 and ICESat-2 during the CRYO2ICE campaign have been compared for a full year using three ICESat-2 models: ATL12, the model based on the individual surface waves, and a baseline model using the standard deviations. The CryoSat-2 data have been compared with data from in situ stations to validate the observations, and the comparison with ICESat-2 has been done with this corrected data. A comparison of CryoSat-2 and Sentinel-3A/B and SARAL has also been done; it shows good agreement between the altimeters. The data have been sorted to find coincident orbit segments for CryoSat-2 and ICESat-2 that contain ocean observations from the Pacific or Atlantic oceans, including the Bering Sea.

In these regions, we found good agreement between the models, with a correlation for ATL12 from ICESat-2 of 0.97, and the standard deviation model had a similar correlation; however, the histogram model is more scattered, with a correlation of 0.95. The models were compared to CryoSat-2 to analyze differences in their behavior, and while the mean deviation of ATL12 was negatively biased compared to CryoSat-2, it had a small RMSE of 0.29 m, while the more scattered histogram model had an RMSE of 0.42 m. The histogram model based on the measured waves experienced a larger positive deviation (0.18 m) at low SWHs (0–1.5 m) and a larger spread than the other models; however, it did have an RMSE in line with a previous analysis [3]. The number of observations at high SWHs (>8 m) is low, and so the behavior of the models is not well-determined for high SWHs.

While ICESat-2 and CryoSat-2 have a smaller correlation, due to the time difference between measurements (2.3 h to 3 h), than comparisons performed for smaller time lags (below one hour), this is in line with the known decrease of the correlation that occurs for longer time lags. Based on the comparison at coincident orbits with CryoSat-2, it can be seen that ICESat-2 is able to provide important additional information about the ocean surface that can be used along with information from conventional altimeters, but it is sensitive to the observation conditions.

Author Contributions: Conceptualization, B.N., O.B.A., H.R. and M.L.R.; methodology, B.N.; software, B.N.; validation, B.N.; formal analysis, B.N.; supervision, O.B.A. and H.R.; investigation, B.N.; resources, O.B.A. and H.R.; data curation, B.N.; writing—original draft, B.N.; writing—review and editing, B.N., O.B.A. and H.R.; visualization, B.N.; project administration, B.N. and O.B.A.; funding acquisition, O.B.A. All authors have read and agreed to the published version of the manuscript.

Funding: This research received no external funding.

Institutional Review Board Statement: Not applicable.

Informed Consent Statement: Not applicable.

Data Availability Statement: CryoSat-2 RADS data are accessible on the DEOS: Rads website: http://rads.tudelft.nl/rads/data/authentication.cgi (accessed on 26 August 2021). Sentinel-3A/B and SARAL RADS data are accessible on the DEOS: Rads website as well (accessed on 10 January 2022). In situ data from the North West Shelf Data Portal are accessible on the website http://nwsportal.bsh.de/ (accessed on 10 January 2022). NASA's ICESat-2 data can be downloaded from the NSIDC website. ATL03: https://nsidc.org/data/ATL03 (accessed on 26 August 2021). ATL12: https://nsidc.org/data/atl12 (accessed on 26 August 2021).

Acknowledgments: We thank the NASA National Snow and Ice Data Center (NSIDC) and the Radar Altimeter Database System (RADS) for distributing the satellite altimetry data, and the North West Shelf Data Portal for the in situ data. We would also like to thank the reviewers for their feedback, which helped improve this paper.

Conflicts of Interest: The authors declare no conflict of interest.

Abbreviations

The following abbreviations are used in this manuscript:

ATLAS	Advanced Topographic Laser Altimeter System
ATL03	ATLAS Global Geolocated Photon Data
ATL12	ATLAS Ocean Surface Height
CDF	Cumulative distribution function
m_0	Variance of surface heights
NOAA	National Oceanic and Atmospheric Administration
NSIDC	National Snow and Ice Data Center
PDF	Probability density function
RADS	Radar Altimeter Database System
RMSE	Root mean squared error
SAR	Synthetic aperture radar
SD	Standard deviation
SI	Scatter index
SIRAL	SAR Interferometric Radar Altimeter
SWH	Significant wave height

Appendix A. In Situ Stations

Table A1. In situ stations used in the validation of CryoSat-2, as well as their locations and local depths.

Station Name	Location [lon E/lat N]	Region	Depth [m]
6200001	−5.00/45.20	Bay of Biscay	4607
6200095	−15.86/52.02	North Atlantic	3295
6400045	−11.40/59.10	North Atlantic	2014
6400046	−4.50/60.70	North Atlantic	1100
Sleipner-A	1.91/58.37	North Sea	96

References

1. Young, I.R. *Wind Generated Ocean Waves*; Elsevier: Amsterdam, The Netherlands, 1999; Volume 2, pp. 1–2, 25–27.
2. Zieger, S.; Vinoth, J.; Young, I.R. Joint calibration of multiplatform altimeter measurements of wind speed and wave height over the past 20 years. *J. Atmos. Ocean. Technol.* **2009**, *26*, 2549–2564. [CrossRef]
3. Klotz, B.W.; Neuenschwander, A.; Magruder, L.A. High-resolution ocean wave and wind characteristics determined by the ICESat-2 land surface algorithm. *Geophys. Res. Lett.* **2020**, *47*, e2019GL085907. [CrossRef]
4. Chelton, D.B.; Ries, J.C.; Haines, B.J.; Fu, L.L.; Callahan, P.S. *Satellite Altimetry and Earth Sciences*; Academic Press: Cambridge, MA, USA, 2001; Volume 69, pp. 1–131.
5. Vignudelli, S.; Kostianoy, A.G.; Cipollini, P.; Benveniste, J. *Coastal Altimetry*; Springer Science & Business Media: Berlin/Heidelberg, Germany, 2011; pp. 1–8.
6. European Space Agency. CryoSat-2 Product Handbook. Available online: https://earth.esa.int/documents/10174/125272/CryoSat-Baseline-D-Product-Handbook (accessed on 15 August 2021).
7. Markus, T.; Neumann, T.; Martino, A.; Abdalati, W.; Brunt, K.; Csatho, B.; Farrell, S.; Fricker, H.; Gardner, A.; Harding, D.; et al. The Ice, Cloud, and land Elevation Satellite-2 (ICESat-2): Science requirements, concept, and implementation. *Remote Sens. Environ.* **2017**, *190*, 260–273. [CrossRef]
8. Morison, J.H.; Hancock, D.; Dickinson, S.; Robbins, J.; Roberts, L.; Kwok, R.; Palm, S.P.; Smith, B.; Jasinski, M.F.; ICESat-2 Science Team. *ATLAS/ICESat-2 L3A Ocean Surface Height, Version 4*; NASA National Snow and Ice Data Center Distributed Active Archive Center: Boulder, CO, USA, 2021. [CrossRef]
9. Kwok, R.; Markus, T. Potential basin-scale estimates of Arctic snow depth with sea ice freeboards from CryoSat-2 and ICESat-2: An exploratory analysis. *Adv. Space Res.* **2018**, *62*, 1243–1250. [CrossRef]
10. Kwok, R.; Kacimi, S.; Webster, M.A.; Kurtz, N.T.; Petty, A.A. Arctic snow depth and sea ice thickness from ICESat-2 and CryoSat-2 freeboards: A first examination. *J. Geophys. Res. Ocean.* **2020**, *125*, e2019JC016008. [CrossRef]
11. Marsh, J.; Webb, E.; Cryosat QC Team. CryoSat CRYO2ICE Orbit Raising Campaign QA4EO QC Summary. Available online: https://earth.esa.int/eogateway/documents/20142/37627/CRYO2ICE-Orbit-Raising-Summary.pdf (accessed on 3 August 2021).
12. Sanchez, J.; Marc, X.; Clerigo, I.; Badessi, S.; Bouffard, J.; Hoyos, B.; Casal, T.; Andreoli, F.; Fornarelli, D.; Albini, G.; et al. Introduction to CryoSat-2 ICESat-2 Resonant Orbits. Available online: https://earth.esa.int/eogateway/documents/20142/37627/Introduction-CryoSat-2-ICESat-2-Resonant-Orbits.pdf (accessed on 15 July 2021).

13. Bagnardi, M.; Kurtz, N.T.; Petty, A.A.; Kwok, R. Sea surface height anomalies of the Arctic Ocean from ICESat-2: A first examination and comparisons with CryoSat-2. *Geophys. Res. Lett.* **2021**, *48*, e2021GL093155. [CrossRef]
14. Neumann, T.A.; Brenner, A.; Hancock, D.; Robbins, J.; Saba, J.; Harbeck, K.; Gibbons, A.; Lee, J.; Luthcke, S.B.; Rebold, T.; et al. *ATLAS/ICESat-2 L2A Global Geolocated Photon Data, Version 4*; NASA National Snow and Ice Data Center Distributed Active Archive Center: Boulder, CO, USA, 2021. [CrossRef]
15. Morison, J.; Hancock, D.; Dickinson, S.; Robbins, J.; Roberts, L.; Kwok, R.; Palm, S.; Smith, B.; Jasinski, M.; Plant, B.; et al. Algorithm Theoretical Basis Document (ATBD) for Ocean Surface Height Version 4. Available online: https://nsidc.org/sites/nsidc.org/files/technical-references/ICESat2_ATL12_ATBD_r004.pdf (accessed on 26 August 2021).
16. Morison, J.; Dickinson, S.; Hancock, D.; Roberts, L.; Robbins, J. Ice, Cloud, and Land Elevation Satellite-2 (ICESat-2) ATL12 Ocean Surface Height Release 004 Application Notes and Known Issues. Available online: https://nsidc.org/sites/nsidc.org/files/technical-references/ICESat2_ATL12_Known_Issues_v004.pdf (accessed on 26 August 2021).
17. Scharroo, R. RADS User Manual. Available online: https://github.com/remkos/rads/raw/master/doc/manuals/rads4_user_manual.pdf (accessed on 26 August 2021).
18. Scharroo, R.; Leuliette, E.W.; Lillibridge, J.L.; Byrne, D.; Naeije, M.C.; Mitchum, G.T. RADS: Consistent multi-mission products. In *Symposium on 20 Years of Progress in Radar Altimetry*; ESA: Venice, Italy, 2012; pp. 5–8. Available online: https://ui.adsabs.harvard.edu/abs/2013ESASP.710E..69S/abstract (accessed on 26 August 2021).
19. Scharroo, R.; Smith, W.; Leuliette, E.; Lillibridge, J. The Performance of CryoSat-2 as an Ocean Altimeter. Available online: https://ui.adsabs.harvard.edu/abs/2012AGUFM.C54A..05S (accessed on 18 September 2021).
20. Bundesamt Für Seeschiffahrt und Hydrographie. North West Shelf Data Portal. Available online: http://nwsportal.bsh.de/ (accessed on 15 May 2021).
21. Alford, J.; Ewart, M.; Bizon, J.; Easthope, R.; Gourmelen, N.; Parrinello, T.; Bouffard, J.; Michael, C.; Meloni, M. #CRYO2ICE Coincident Data Explorer, Version 1. Available online: http://cryo2ice.org (accessed on 10 August 2021).
22. Casas Prat, M. Overview of Ocean Wave Statistic. Available online: https://upcommons.upc.edu/handle/2099.1/6034 (accessed on 15 August 2021).
23. Ranndal, H.; Christiansen, P.S.; Kliving, P.; Andersen, O.B.; Nielsen, K. Evaluation of a statistical approach for extracting shallow water bathymetry signals from ICESat-2 ATL03 photon data. *Remote Sens.* **2021**, *13*, 3548. [CrossRef]
24. Scharroo, R. RADS Data Manual. Available online: https://github.com/remkos/rads/raw/master/doc/manuals/rads4_data_manual.pdf (accessed on 26 August 2021).